

AN X-RAY/OPTICAL STUDY OF THE COMPLEX DYNAMICS OF THE CORE OF THE MASSIVE INTERMEDIATE-REDSHIFT CLUSTER MACSJ0717.5+3745

CHENG-JIUN MA, HARALD EBELING, AND ELIZABETH BARRETT

Institute for Astronomy, University of Hawaii, 2680 Woodlawn Drive, Honolulu, HI 96822, USA

Received 2008 August 20; accepted 2009 January 26; published 2009 February 17

ABSTRACT

Using *CHANDRA*, we investigate the spatial temperature distribution of the intracluster medium (ICM) within 700 kpc of the center of the massive merging cluster MACSJ0717.5+3745 at $z = 0.55$. Combining the X-ray evidence with information about the distribution and velocities of the cluster galaxies near the core provides us with a snapshot of the three-dimensional geometry and dynamics of one of the most complex clusters studied to date. We find MACSJ0717.5+3745 to be an active triple merger with ICM temperatures exceeding 20 keV. Although radial velocity information and X-ray/optical offsets indicate that all three mergers proceed along distinctly different directions, the partial alignment of the merger axes points to a common origin in the large-scale filament south-east of the cluster core. Clear decrements in the ICM temperature observed near two of these subclusters identify the respective X-ray surface brightness peaks as remnants of cool cores; the compactness and low temperature of 5.7 keV of one of these features suggest that the respective merger, a high-velocity collision at $3,000 \text{ km s}^{-1}$, is still in its very early stages. Looking beyond the triple merger, we find the large-scale filament to not only provide a spatial as well as temporal arrow for the interpretation of the dynamics of the merger events near the cluster core, but we also find tantalizing, if circumstantial, evidence for direct, large-scale heating of the ICM by contiguous infall of low-density gas from the filament.

Key words: galaxies: clusters: individual (MACSJ0717.5+3745) – X-rays: galaxies: clusters

1. INTRODUCTION

Major cluster mergers are the most energetic events in the universe, and one of the most important phenomena for the formation of large-scale structure in the hierarchical scenario. The enormous energy released in cluster mergers accelerates particles to relativistic energies and can, in the most massive systems, heat the intracluster medium (ICM) to temperatures exceeding 20 keV (see the review by Sarazin 2002). In an astrophysical context, dynamically simple two-component mergers like 1ES0657–56 have been instrumental in obtaining the currently best constraint on the self-interaction cross section of dark matter (Markevitch et al. 2004; Randall et al. 2008).¹ Few mergers, however, are as straightforward to interpret as 1ES0657–56 which consists of only two well separated components, and whose merger axis is almost perpendicular to our line of sight. While the majority of massive mergers are thus among the most challenging systems for studies of the dynamics and interactions of gas, galaxies, and dark matter, they also offer the greatest opportunity to study, with good statistics, the full complexity of cluster mergers.

A prime example of a complex, major cluster merger is MACSJ0717.5+3745 ($z = 0.545$). Discovered during the massive cluster survey (MACS; Ebeling et al. 2001, 2007), the system is one of the most X-ray luminous and best-studied massive clusters at intermediate redshifts. The wealth of data accumulated for it from X-ray to mm wavelengths make MACSJ0717.5+3745 a promising target for a comprehensive study of the full range of physical mechanisms at work during the assembly of massive clusters. At radio frequencies, synchrotron emission from relativistic electrons in MACSJ0717.5+3745 was detected in the form of both a radio halo and a very extended, steep-spectrum radio relic (Edge et al. 2003). The same

relativistic electrons are expected to also produce hard X-ray photons via inverse Compton scattering of cosmic microwave background photons, as reported by Petrosian et al. (2006). The spatial distribution of the galaxy population in and around MACSJ0717.5+3745 was studied by Ebeling et al. (2004) who found the cluster to be connected to an extended linear filamentary structure, consistent with the picture seen in numerical simulations (and observationally supported by the findings of Kartaltepe et al. 2008) that the most massive halos are more likely to be surrounded by pronounced large-scale structure (e.g. Colberg et al. 2000, 1999). Finally, a spectroscopic analysis by Ma et al. (2008) found strong evidence for star formation in many galaxies in and around this cluster, likely caused by the ongoing growth of this complex system. In this Letter, we study variations in the temperature of the ICM of MACSJ0717.5+3745 and their correlation with features in the spatial and radial velocity distribution of the cluster galaxy distribution, in order to assess the dynamical state and history of the cluster core.

2. X-RAY DATA

MACSJ0717.5+3745 was observed with the *Chandra* Advanced CCD Imaging Spectrometer Imaging array (ACIS-I; Garmire et al. 2003) in 2003 January for a total exposure time of 60 ks in VFaint mode (ObsID 4200). We applied standard *Chandra* data reduction procedures² to reprocess the event file using CIAO 3.3.0.1 and CALDB 3.2.1. Our spectroscopic analysis made use of a “blank-sky” background file³ to remove low-level soft X-ray emission covering a majority of the ACIS-I array.

An adaptively smoothed representation of the data within the full field of view of ACIS-I is shown in Figure 1. The disturbed X-ray morphology around the core of the cluster,

¹ See also Mahdavi et al. (2007) and Bradač et al. (2008) for results obtained for A 520 and MACSJ0025.4–1222.

² http://cxc.harvard.edu/ciao/guides/acis_data.html.

³ See <http://cxc.harvard.edu/contrib/maxim/acisbg/COOKBOOK>.

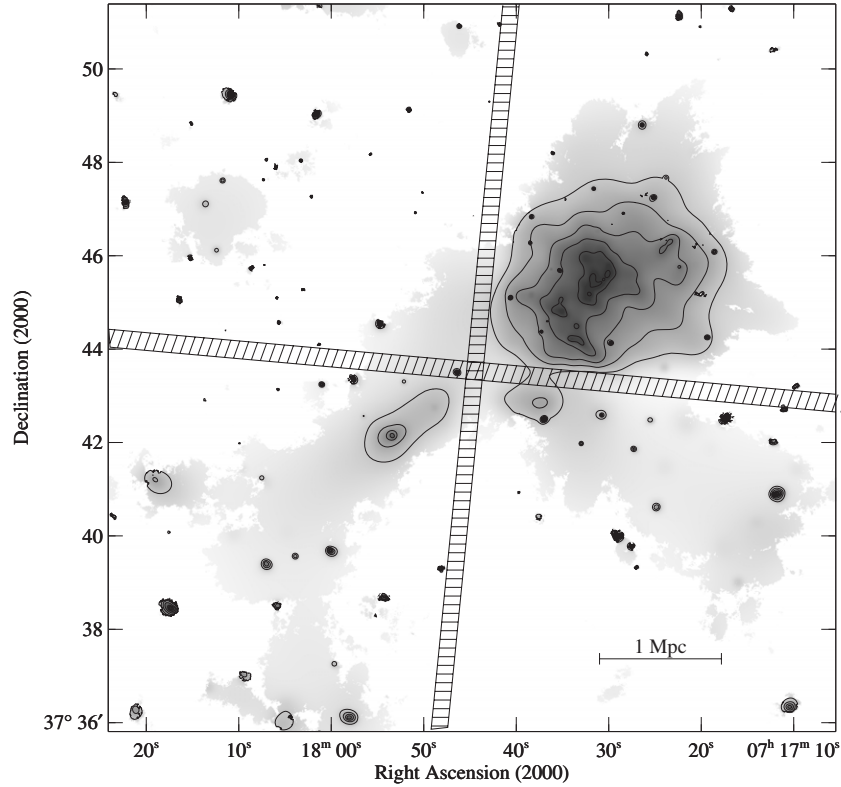


Figure 1. X-ray emission in the field of MACSJ0717.5+3745 as observed with the *Chandra* ACIS-I detector in the 0.5–7 keV band. The image has been weighted by the exposure map and adaptively smoothed using the *asmooth* algorithm (Ebeling et al. 2006) requiring a minimal significance of 99% with respect to the local background (see also Ma et al. 2008; Ebeling et al. 2007). The shaded region marks the chip gaps. Contours are logarithmically spaced by factors of 2, starting at six times the value of the global X-ray background.

which contains at least four X-ray surface-brightness peaks, is immediately obvious in the upper right corner. In addition, weak but detectable X-ray emission extends to the south-eastern corner of Figure 1, matching the large-scale filament discovered in the galaxy distribution by Ebeling et al. (2004).⁴

3. OPTICAL DATA

MACSJ0717.5+3745 was observed with the Advanced Camera for Surveys (ACS) aboard the *Hubble Space Telescope* (*HST*) in the F555W and F814W passbands on 2004 April 2 for an effective exposure time of 4470 s and 4560 s, respectively, as part of a comprehensive *HST* survey of the most distant MACS clusters (GO-09722). Groundbased observations of the galaxy population of the cluster were conducted with Keck-II/DEIMOS from 2004 to 2008 with the aim of probing large-scale cluster dynamics and examining the effect of environment on galaxy evolution (Ma et al. 2008).

4. X-RAY TEMPERATURE MAP

As is apparent from its complex X-ray morphology, MACSJ0717.5+3745 is far from virialized, and the gas temperature can be expected to vary significantly in its core.⁵ In order to derive a spatial temperature map, we need to define suitable regions for X-ray spectroscopy.⁶ Ideally, these regions

should follow the temperature structure. The latter, however, is a priori unknown, and the limited photon statistics of our data do not allow us to extract spectra in arbitrarily small bins. We address this problem by adopting a two-level binning method. As a first step, we subdivide the image into regions whose shape is guided by the X-ray surface-brightness distribution, and each of which contains enough photons to allow a crude temperature measurement. We then merge adjacent regions with similar temperature in order to obtain a clearer view of temperature variations on larger scales. This procedure ensures that the final regions represent the temperature structure fairly, and also that the resulting measurements are statistically robust.

4.1. Low-Fidelity Temperature Map

The initial regions for this process are determined by running the “accumulative binning” algorithm *contbin* (Sanders 2006) on the exposure-weighted image.⁷ We chose *contbin* because the algorithm’s choice of bins is physically motivated, in as much as *contbin* attempts to follow the X-ray surface brightness, which is related to the ICM temperature and density. If the initial regions are sufficiently small, their choice will, by the end of the merging process, not affect the final temperature map.

The results of this first-level binning step are shown in the top two panels of Figure 2. As expected, the relatively low signal-to-noise ratio (S/N) chosen leads to large errors in the measured temperatures and to low χ^2 values of ~ 0.6 . Although the best-fit temperatures for some regions, mostly the hottest ones, are

⁴ This includes the satellite cluster 2 Mpc southeast (SE) of the main system; we measure its ICM temperature to be 2.7 ± 0.3 keV.

⁵ A summary of the *global* properties of the hot gas in MACSJ0717.5+3745 is given by Ma et al. (2008).

⁶ We perform all spectral fitting with *Sherpa* using a MEKAL plasma model (Mewe et al. 1985), with the absorption term fixed at the Galactic value of $n_H = 7.11 \times 10^{20} \text{ cm}^{-2}$, the redshift of the cluster set to $z_{cl} = 0.5446$ (Ma et al. 2008), and abundance $Z = 0.3Z_\odot$.

⁷ In *contbin* the image was smoothed to a S/N of 10, and we set the “constraint parameter” C (Sanders 2006) to 1.5 to prevent the bins from becoming too elongated. The S/N required of the resulting regions was 20, which corresponds to 400 net counts in regions with negligible background.

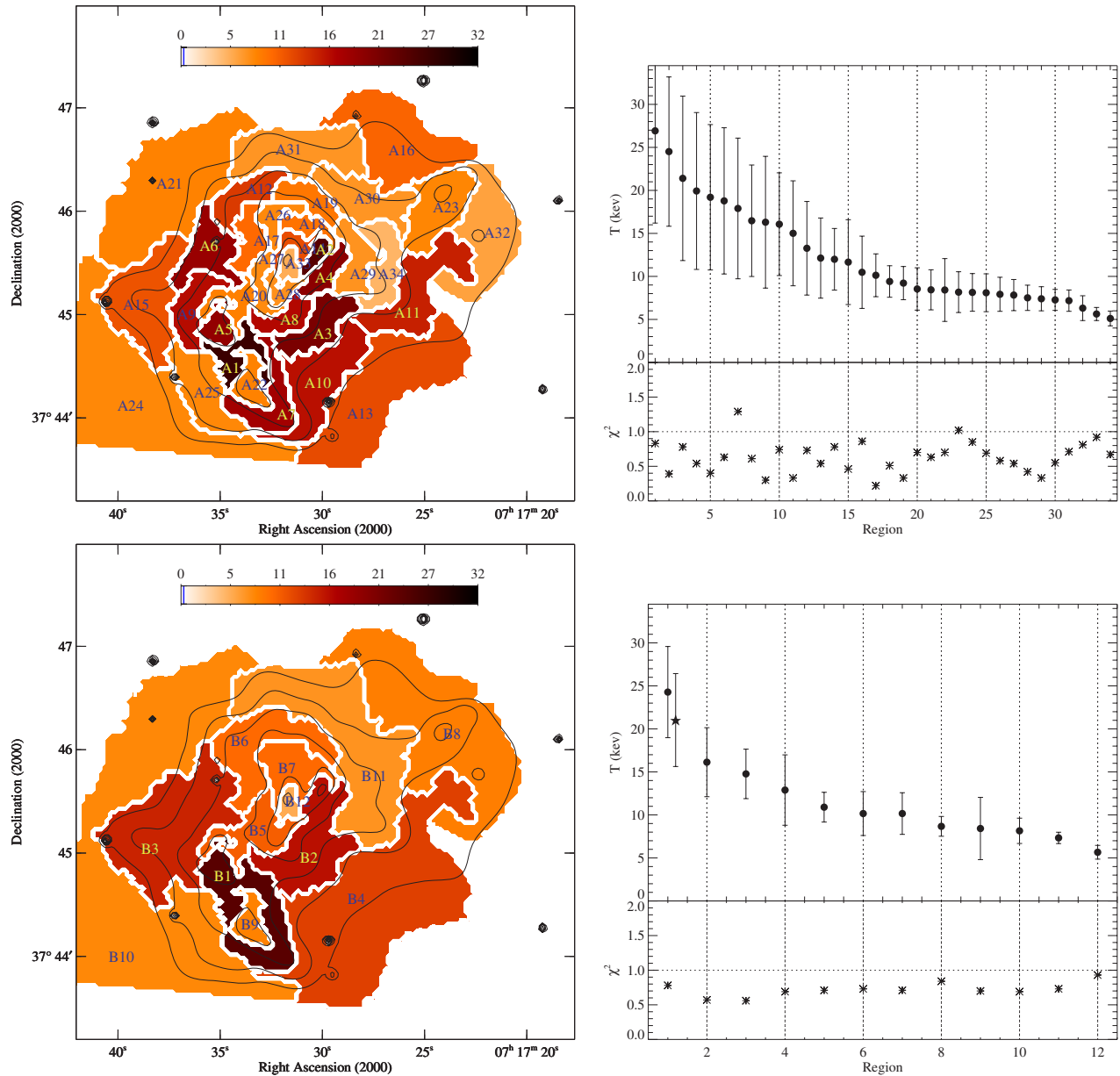


Figure 2. Left panels: X-ray temperature maps from our two-step binning process. The temperature is coded as indicated by the color bar. Right panels: the best-fit temperature and reduced χ^2 value for each bin. Top: results for the initial regions generated by *contbin*. Bottom: results for regions created in the subsequent rebinning process. The second temperature shown for region B1 (open circle) is the result obtained when the embedded cool region B9 is included.

poorly constrained, we already see clear variations and trends of the ICM temperature within our study region.

4.2. Re-Binning

As a second step, we examined the temperature map from Stage 1 and combined adjacent regions with similar temperature in order to obtain a clearer view of temperature variations on larger scales, the goal being to reach at least 1200 net counts per bin by combining three (occasionally four) of the initial regions. The results of this rebinning process are shown in the bottom two panels of Figure 2; the individual regions and their temperatures are listed in Table 1.

Note that two of the initial regions were excluded from the rebinning and left unchanged, namely the ones coinciding with the main peaks in the X-ray surface brightness distribution, A22 (B9) and A33 (B12). Both of these exhibit markedly cooler temperatures than their surroundings, making them likely candidates for cool cores of clusters still in the process of

Table 1
Results from Spectral Fitting

Region	kT ^a (keV)	χ^2	Binning Table
B1	24.3 ± 5.3	0.78	A1, A5, A7
B2	16.1 ± 4.0	0.57	A2, A3, A4, A8
B3	14.8 ± 2.9	0.56	A6, A9, A15
B4	12.9 ± 4.1	0.69	A10, A11, A13
B5	10.9 ± 1.7	0.71	A20, A27, A28
B6	10.2 ± 2.5	0.73	A12, A17, A19
B7	10.2 ± 2.4	0.71	A14, A18, A26
B8	8.7 ± 1.2	0.84	A16, A23, A32
B9	8.4 ± 3.6	0.70	A22
B10	8.2 ± 1.5	0.69	A21, A24, A25
B11	7.3 ± 0.7	0.73	A29, A30, A31, A34
B12	5.7 ± 0.8	0.93	A33

Note. ^a The quoted errors denote 1σ uncertainty.

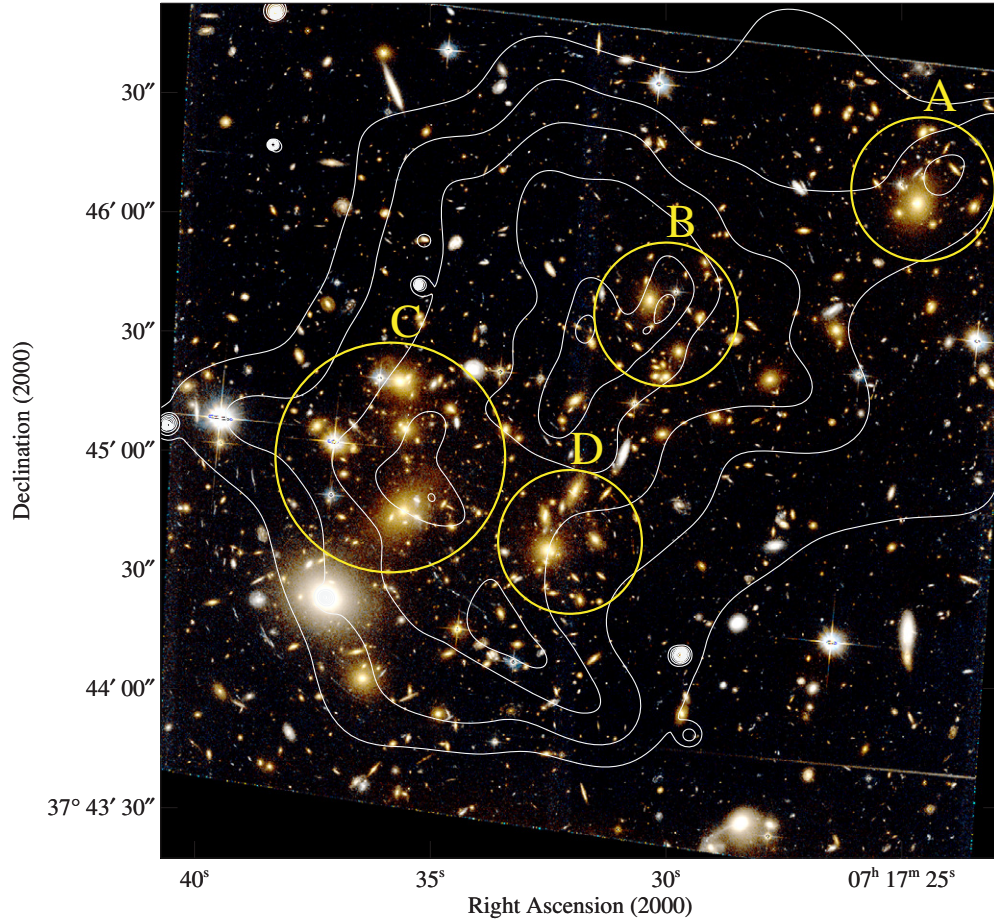


Figure 3. X-ray contours as in Figure 2 overlaid on the F555W/F814W optical image of the cluster core obtained with *HST*/ACS. Yellow circles centered on the four main peaks in the cluster light distribution mark the regions within which average radial velocities and velocity dispersions were computed for the enclosed galaxies (see Table 2).

Table 2
Average Radial Velocities and Velocity Dispersions for Galaxies in the Regions Marked in Figure 3

Label	Number of Redshifts	ΔV^a (km sec ⁻¹)	σ^a (km sec ⁻¹)
A	10	278^{+295}_{-339}	1021^{+139}_{-318}
B	9	3238^{+252}_{-242}	664^{+63}_{-304}
C	10	-733^{+486}_{-478}	1761^{+234}_{-607}
D	7	831^{+843}_{-800}	1328^{+968}_{-424}

Note. ^a Calculated using the bootstrap estimator in Beers et al. (1990).

merging with the main system. This interpretation is particularly plausible for the region around the global peak in the X-ray emission from MACSJ0717.5+3745, A33 (B12), which is found to contain the coolest gas anywhere within our study region ($kT = 5.7 \pm 0.8$ keV). By comparison, the temperature measured for the second putative cool core, region A22 (B9), is much higher and less well constrained ($kT = 8.4 \pm 3.6$ keV), but still in stark contrast to the much higher temperatures above 15 keV measured in its immediate vicinity (regions A1, A5, and A7). With all of these regions being viewed in projection, the true temperature difference is likely to be yet higher. Better constraints from a two-phase plasma model, especially relevant for region B9, would require significantly better photon statistics.

Although the selection of regions to merge is to some degree subjective, we convinced ourselves that our final results and conclusions are robust. For instance, our perhaps most debatable choice, the exclusion of the aforementioned cool core A22 (B9) from the merging of the surrounding regions A1, A5, and A7 (B1), predictably increases the temperature measured for B1 ($kT = 24.3 \pm 5.3$ keV); including it, however, still leads to a statistically consistent result of $kT = 21.0 \pm 5.4$ keV (Figure 2).

5. CLUSTER GALAXY DISTRIBUTION AND DYNAMICS

Our tentative interpretation of the physical origins of the complex temperature and gas density distribution presented in the previous section can be tested and extended by studying the distribution and dynamics of the cluster galaxies in the same region. Shown in Figure 3 is an overlay of the X-ray contours from Figure 2 onto the *HST* image of the cluster core. We identify four major concentrations in the integrated optical light, which is dominated by the large cluster ellipticals. Average redshifts and velocity dispersions for galaxies within the four circles marked in Figure 3 are listed in Table 2. Unlike their counterparts in regions A, C, and D, the galaxies associated with feature B are found to move through the cluster core at a very high relative radial velocity of over 3,000 km s⁻¹, close to the maximal velocity expected from infall from infinity. No significant differences are found between the velocity dispersions measured for the four regions, although the results suggest that the structure in region C is the most massive one.

6. INTERPRETATION

A comparison of the gas and galaxy distribution shown in Figure 3 as well as of the radial velocity information summarized in Table 2 yields important insights into the dynamics of the multiple components of the cluster core. Specifically, we note that, of the four galaxy concentrations discussed in Section 5, only A and C are reasonably well aligned with peaks in the X-ray surface brightness. The good X-ray/optical alignment of component C, combined with a systemic velocity and velocity dispersion consistent with those of MACSJ0717.5+3745 as a whole, makes this subsystem a likely candidate for the actual, if disturbed, core of the main cluster.

The dominant galaxies in regions B and D, on the other hand, are offset by about 25 arcsec (~ 160 kpc at the cluster redshift) from the respective X-ray peak—in both cases in a direction that points toward the filament to the SE of the main cluster. Offsets of this kind between gas and galaxies (and dark matter) have been observed before in merging clusters, examples being the Bullet Cluster 1ES0657–56 (Markevitch et al. 2004) and MACSJ0025.4–1222 (Bradač et al. 2008), and are readily explained by the difference in the self-interaction cross sections of the various cluster constituents. The X-ray temperature maps of Figure 2 show the gas near regions B and D being cool compared to their surroundings (B9 and B12); we can thus safely identify them as the cool cores of clusters merging with the main body of MACSJ0717.5+3745 and falling behind as their respective galaxy populations advance. While the merger axis of system D is consistent with lying in the plane of the sky (and aligned with the large-scale filament prominently visible on the left of Figure 1), the combination of the observed X-ray/optical offset with a very high radial velocity indicates that system B is moving through the cluster core along an axis that is much more inclined toward our line of sight. We note also that the high-velocity collision of component B most likely happened only recently, given that its cool core (region B12 in Figure 2) appears to be still largely intact.

A similar argument can be made to explain the observational evidence in region A. The X-ray/optical offset suggests infall from the northwest (NW), i.e. in the direction of the filament. The trailing peak in the gas density is highly elongated though, and no cool gas is detected in the area, all of which suggests that we are witnessing back-infall of a cluster that originated from the filament and has already passed through the main cluster once.

While the combined X-ray/optical evidence allows a straightforward and self-consistent interpretation of the dynamics and three-dimensional geometry of the three separate ongoing merger events described above, the gas distribution and

temperature structure near the cluster–filament interface—the south-eastern corner of Figures 2 and 3—defies simple explanation. Although the extremely high temperatures measured in regions B1 and B2 could to some extent be caused by shock heating from the ongoing mergers of components B and D, this explanation appears implausible for the entirety of the hot interface region extending from B3 to B4. The sheer size of this feature (about 1 Mpc), its alignment perpendicular to the cluster–filament axis, and the simultaneous increase in gas temperature and X-ray surface brightness all point to a direct large-scale interaction between the filament and the cluster core. We therefore speculate that the prominent jump in gas density and temperature along the cluster–filament interface is the result of contiguous accretion of gas along the large-scale filament feeding MACSJ0717.5+3745. A deeper *Chandra* observation would allow this hypothesis to be tested and may yield the first credible characterization of the gas content of large-scale filaments.

We thank Phil Marshall and the *HST* Archive Galaxy-scale Gravitational Lens Survey (HAGGLEs) team for making their reprocessed *HST* images of MACSJ0717.5+3745 available for this study. We are also indebted to an anonymous referee whose criticism led to substantial improvements of this paper. Last, but not least, we gratefully acknowledge financial support by NASA grant NAG 5-8253, SAO grant GO3-4168X, and STScI grant GO-09722.

REFERENCES

- Beers, T. C., Flynn, K., & Gebhardt, K. 1990, *AJ*, **100**, 32
- Bradač, M., et al. 2008, *ApJ*, **687**, 959
- Colberg, J. M., et al. 1999, *MNRAS*, **308**, 593
- Colberg, J. M., et al. 2000, *MNRAS*, **319**, 209
- Ebeling, H., Barrett, E., & Donovan, D. 2004, *ApJL*, **609**, 49
- Ebeling, H., Edge, A., & Henry, P. 2001, *ApJ*, **553**, 668
- Ebeling, H., White, D., & Rangarajan, F. 2006, *MNRAS*, **368**, 65
- Ebeling, H., et al. 2007, *ApJL*, **661**, 33
- Edge, A. C., et al. 2003, *MNRAS*, **339**, 913
- Garmire, G. P., et al. 2003, *Proc. SPIE*, **4851**, 28
- Ma, C.-J., et al. 2008, *ApJ*, **684**, 160
- Kartaltepe, J., Ebeling, H., Ma, C.-J., & Donovan, D. 2008, *MNRAS*, **389**, 1240
- Mahdavi, A., et al. 2007, *ApJ*, **668**, 806
- Markevitch, M., et al. 2004, *ApJ*, **606**, 819
- Mewe, R., Gronenschild, E. H. B. M., & van den Oord, G. H. J. 1985, *A&AS*, **62**, 197
- Petrosian, V., Madejski, G., & Luli, K. 2006, *ApJ*, **652**, 948
- Randall, S. W., et al. 2008, *ApJ*, **679**, 1173
- Sanders, J. S. 2006, *MNRAS*, **371**, 829
- Sarazin, C. L. 2002, in *Merging Processes in Galaxy Clusters*, ed. L. Feretti, I. M. Gioia, & G. Giovannini (Dordrecht: Kluwer), 272, 1